Available online at www.sciencedirect.com
SCIENCE DIRECT®
Ocean Modelling 7 (2004) 145–163
Ocean Modelling
www.elsevier.com/locate/ocemod

Tropical instability waves in the Atlantic Ocean

Markus Jochum *, Paola Malanotte-Rizzoli, Antonio Busalacchi

MIT/WHOI Joint Program, Earth, Atmospheric, Planetary Sciences, 77 Massachusetts Avenue, Room 54-1410, Cambridge, MA 02138, USA

Received 25 February 2003; received in revised form 29 May 2003; accepted 1 July 2003

Abstract

An idealized numerical model of the tropical Atlantic Ocean is used to study the structure, energetics and heat flux of the Atlantic tropical instability waves (TIWs). The model results compare well with the observations, and they both show that, unlike commonly assumed, the TIWs in the Atlantic exist on both sides of the equator and are generated not only in the summer but from May to January. Furthermore it is demonstrated that the Atlantic TIWs are generated by barotropic instability of the shear between the equatorial undercurrent and the northern south equatorial current and make a surprisingly small contribution to the heat budget of the equatorial mixed layer. The model results reveal that the often published strong meridional heat flux divergence of the TIWs is largely compensated for by their vertical heat flux divergence.

1. Introduction

Tropical instability waves (TIWs) are a phenomenon common to both the Atlantic and the Pacific Oceans (Dueing et al., 1975; Legeckis, 1977); the focus of the present study are the TIWs in the Atlantic Ocean. Their surface structure can be seen best in satellite pictures of sea surface temperature (Steger and Carton, 1991) and ocean color (Fig. 1) where they can be observed during summer at 4°S and 4°N as cusp-like features with wavelengths between 600 and 1200 km (Legeckis and Reverdin, 1987; Steger and Carton, 1991). The estimates of phase speed range between 20 and 50 cm/s[1]. Apart from being seen in optical satellite observations, TIWs have been found in the sea surface height signal of Geosat (Musman, 1992) and TOPEX/POSEIDON (Katz, 1997). Both their estimates of phase speed and wavelength are consistent with the results of

* Corresponding author. Tel.: +1-617-253-3573.
E-mail address: markus@ocean.mit.edu (M. Jochum).

1463-5003/$ - see front matter
doi:10.1016/S1463-5003(03)00042-8

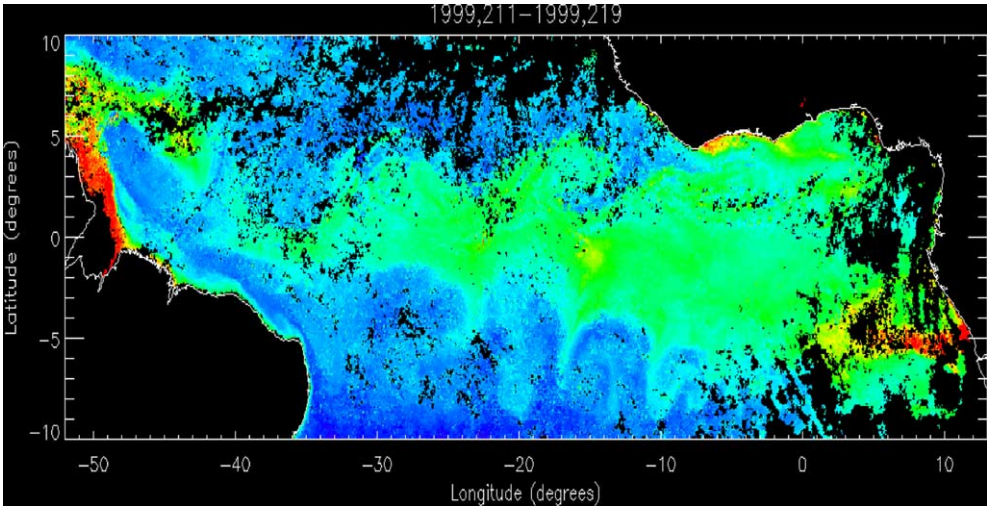

Fig. 1. TIWs as seen by SeaWiFS (courtesy of M. Uz). Note the cusps in ocean color along 4°S and 4°N.

Legeckis and Reverdin (1987) and Steger and Carton (1991). The analysis of ship drift and drifter data confirms the satellite based observations (Richardson and Reverdin, 1987); moreover the analysis by Richardson and Philander (1987) demonstrates that the TIWs are strongest away from the eastern or western boundary, in the center of the basin.

The subsurface structure and the frequency domain of TIWs have been studied with current meter moorings by Weisberg (1984) and Weisberg and Weingartner (1988, WW from here on). The mooring records show that their potential energy is negligible and that their kinetic energy has a central periodicity of approximately 25 days. The energy reaches a maximum of 1600 cm^2/s^2 at the surface and the center of the basin along the equator and decays rapidly below 50 m depth or east of 15°W. Still, signals of TIWs were found as deep as 800 m (Boebel et al., 1999) and as far east as 4°W (Weisberg et al., 1979).

Early analytical studies by Philander (1976, 1978) demonstrate that the equatorial zonal currents are barotropically unstable and preferentially generate waves with wavelengths and periods of the observed TIWs. A series of highly idealized numerical studies corroborated these findings but showed that baroclinic (Cox, 1980), frontal (Yu et al., 1995) and Kelvin–Helmholtz instabilities (Proehl, 1996) can contribute as well. Cox (1980) pointed out that what is simply referred to as TIWs is a superposition of unstable waves and their projection on the set of free equatorial waves. The latest and most thorough study on TIWs and their energetics is provided by Masina and Philander (1999) and Masina et al. (1999). With an idealized numerical model of the Pacific Ocean they show that localized studies of the energy budget might be misleading, the whole equatorial domain has to be analyzed before a definite conclusion about the energy sources and sinks of the TIWs can be reached. This study emphasizes that TIWs cannot be analyzed in general or in isolation, but that the generation, structure and decay of TIWs depends on the particular generation region.

A detailed understanding of the TIWs is necessary because of their potential importance for climate. WW estimate that the equatorward heat flux of the TIWs in the upper 50 m is ap-

proximately 100 W/m^2 which is comparable to the atmospheric heat flux in the tropics. For the Pacific, observations by Hansen and Paul (1984), Bryden and Brady (1989) and model results by Vialard et al. (2001) find even higher values. Thus, the TIWs could have an important influence on the phase of the seasonal cycle and the position of the equatorial cold tongue and the intertropical convergence zone (ITCZ). Furthermore, TIWs have been shown to be important for the oxygen and salinity front in the intermediate waters along the equator (Jochum and Malanotte-Rizzoli, 2003b) and Jochum and Malanotte-Rizzoli (2003a) demonstrated that TIWs drive the south equatorial undercurrent (SEUC). The effect of TIWs on equatorial Atlantic plankton and nutrient distribution has been observed and discussed by Menkes et al. (2002).

The main purpose of the present study is to make a connection between the theoretical ideas developed in previous studies and the actual processes in the Atlantic Ocean. Their short time and length scales and their global importance suggests to study the TIWs with numerical models. However, in the only numerical study of the Atlantic TIWs that the authors are aware of (Philander et al., 1986), the TIWs are strongly damped by high viscosity, and their energetics are not discussed. Here, we present results of a numerical model of the tropical Atlantic whose main difference to the Philander et al. (1986) configuration is the order of magnitude smaller horizontal viscosity. Through a close comparison between model results and observations it is shown that the model adequately represents the observations and can provide a look into the temporal and spatial structure of the TIWs which, in this detail, is not possible with observations alone. Furthermore, the present study quantifies the energetics and the heat flux of the TIWs in the Atlantic Ocean. The plan of the paper is as follows. A detailed comparison between observations and model results is presented in Section 2. This is followed by a discussion of their energetics in Section 3 and an estimate of their heat flux in Section 4. Section 5 provides a summary.

2. Comparison between model results and observations

The model used is the MOM2b code. The domain is an idealized basin from 25°S to 30°N in latitude and from 70°W to 15°E in longitude, with a flat bottom at 3000 m. The resolution is 1/4° by 1/4° at the western boundary between the equator and 12°N, and becomes coarser towards the eastern, northern and southern boundaries: the latitudinal resolution is reduced from 1/4° to 1° at the meridional boundaries, the longitudinal resolution is reduced from 1/4° to 1.5° at the zonal boundaries. There are 30 levels in the vertical with a 10 m resolution in the top 100 m. Horizontal mixing is done by a Laplacian scheme with the eddy viscosity and diffusivity being linearly dependent on the resolution: from 200 m^2/s^1 for 1/4° to 2000 m^2/s^1 for 1° resolution. In the vertical, a Richardson number-dependent vertical mixing scheme is used. The wind forcing is provided by Hellerman and Rosenstein (1983). A detailed discussion of the model setup can be found in Jochum and Malanotte-Rizzoli (2003c), where it is shown that all the simulated currents compare well with the observations. Fig. 2 shows the annual mean zonal flow in the model across 25°W.

For the comparison, mainly two types of data will be considered: satellite based observations which provide information about wavelength and phase speed, and records of current meter moorings which are indispensible to determine the amplitude, period and seasonality of the TIWs. Temperature records from moorings, although more plentiful, were not found to be useful after the authors analyzed the temperature records of the recently recovered PIRATA mooring array

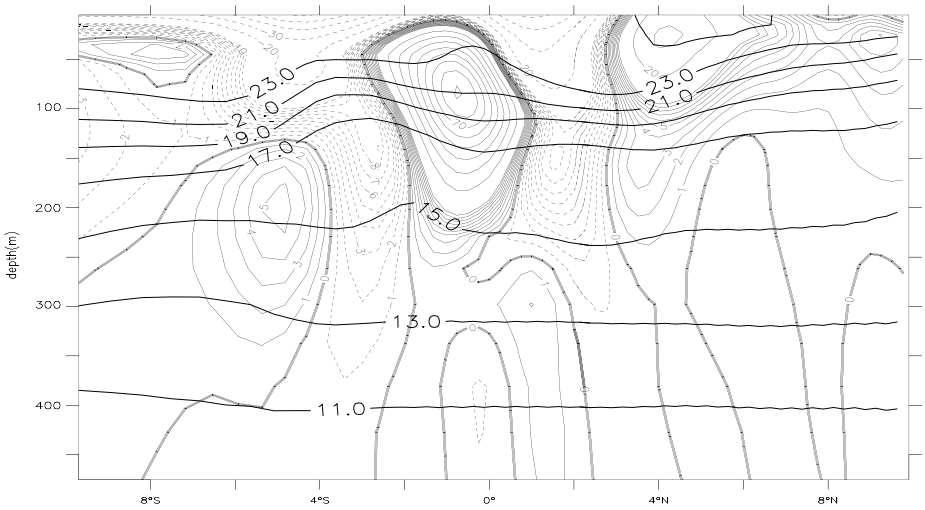

Fig. 2. Simulated annual zonal mean velocity (in cm/s) across 25°W with superimposed isotherms. The eastward currents are contoured with solid lines and are called (from south to north): south equatorial countercurrent (SECC), south equatorial undercurrent (SEUC), equatorial undercurrent (EUC) and north equatorial countercurrent (NECC). The two westward currents, centered at 4°S and 2°N are the southern and northern south equatorial current (sSEC and nSEC).

(www.ifremer.fr/orstom/pirata/pirataus.html). For no location did the temperature variance in the 20–50 day band exceed the noise level. This does not mean that TIWs were not present during the measurement period, rather it shows that TIWs do not have a temperature signal at the equator. In the Pacific, too, the equatorial SST anomalies have been described as rather weak (Chelton et al., 2000; Vialard et al., 2001). The off-equatorial PIRATA moorings are either too far away from the equator or the records are too short to detect a TIW signal.

The satellite based observations mentioned in the introduction report wavelengths between 600 and 1200 km and phase speeds between 20 and 50 cm/s. This large spread of values has observational, theoretical and physical causes. The observational difficulties are different for the altimeter than for the optical instruments. SST and ocean color analyses are obstructed by clouds and background noise whereas observing the TIWs with an altimeter is difficult because of the short time and length scales of the TIWs. For example, the prominent signals south of the equator in Fig. 1 are not matched by any signal in altimetry (Goni, pers. comm.).

A theoretical cause for the large spread is that the concepts of phase speed and wavelength are defined only for free waves. It is difficult to apply theses concepts to growing or decaying waves. A free Rossby wave that enters a region of growth increases its apparent wavelength and phase speed, because the velocity or temperature in the growth region changes not only due to the westward phase speed but also because the wave feeds on the energy of the unstable currents. Thus, the western part of a crest grows faster than the eastern part which gives rise to an increased distance between two adjacent crests. The opposite is true in regions of wave decay. Fig. 3 illustrates both cases. It shows the same wave at two different times 10 days apart. The apparent wavelength and phase speed are much larger in the east, where the wave is growing, than in the west, where the wave is decaying. If the wavelength is the distance between two maxima, then the

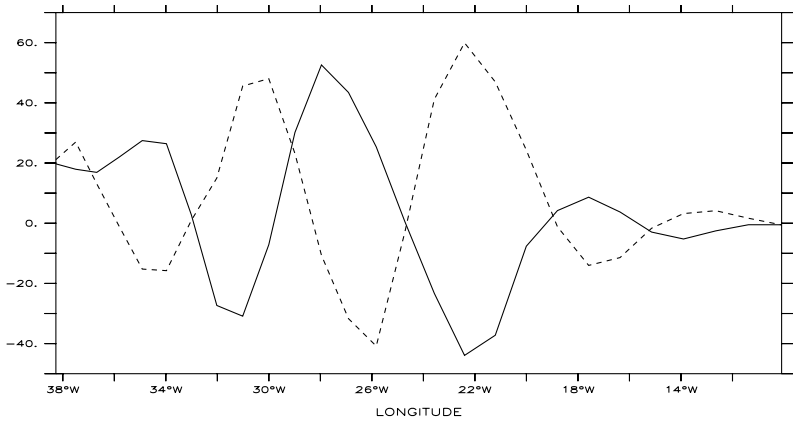

Fig. 3. Simulated meridional velocity (in cm/s) at the surface along the equator at the beginning of June (—) and 10 days later (- - -). The phase speed is westward, the minimum at 22°W moves within 10 days to 26°W.

wavelength would be 700 km in the western part of the basin and 1100 km in the eastern part (Fig. 3). Similarly, by measuring the distance the wave crests cover in 10 days, one can infer from this figure a phase speed of 30 cm/s for the western part and 50 cm/s for the eastern part of the basin. Thus, one would expect the observed spread in phase speed and wavelength from theoretical causes alone.

The physical reason to expect a certain range in the wave properties is that the TIWs are generated by an unstable flow field and not by direct meteorological forcing with a distinct period. Therefore it is possible for the TIW properties to have a range of values, depending on the properties of the most unstable modes. Interestingly, however, Cox (1980) showed in a numerical study that the dominant period and wavelength of the TIWs do not change under a wide range of parameters. Independent of friction and resolution, he finds maximum growth for waves with a period of 30 days and a wavelength of 1200 km. The main changes in his experiments occur after a reduction of viscosity which leads to an increase of wave energy and a spreading of wave energy to adjacent wavenumbers.

The period of the TIWs has been estimated in Weisberg et al. (1987). They find on the equator at 28°W for the meridional velocity a central periodicity of 25 days. This is consistent with the findings of Cox (1980), Philander et al. (1986) and the results of the present study. Fig. 4 shows the spectrum of the meridional velocity in the model on the equator at 28°W. Like in the observations, the spectrum shows a broad peak in energy density between 20 and 50 days with a maximum between 25 and 30 days. The spectra are slightly different at different locations (not shown) but the energy is always concentrated in the 20–50 day band. This analysis shows that the model's representation of the TIWs has periods, wavelengths and phase speeds which are consistent with the observations. It is now proceeded with an analysis of the TIW's amplitudes.

The estimation of the TIW amplitude is based mainly on the records of the current meter moorings from the SEQUAL (Seasonal Response of the Equatorial Atlantic) and FOCAL (Francais Ocean et Climat dans l'Atlantic Equatorial) programs. The programs took place during the transition from the 1983 El Niño to the 1984 La Niña (Hisard et al., 1986). The resulting interannual variability in the wind fields leads to interannual variability in the background states

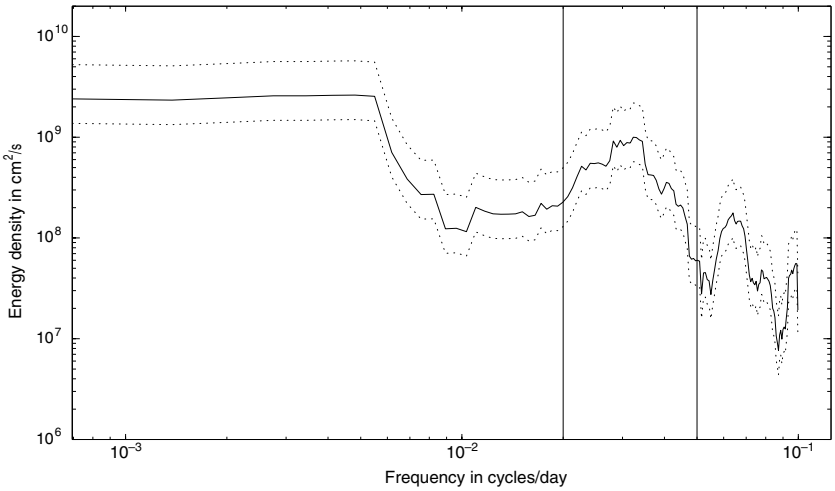

Fig. 4. Spectrum of the meridional velocity at the surface at the equator at 28°W. The 95% confidence interval is indicated by the dotted line, the vertical lines indicate periods of 20 and 50 days.

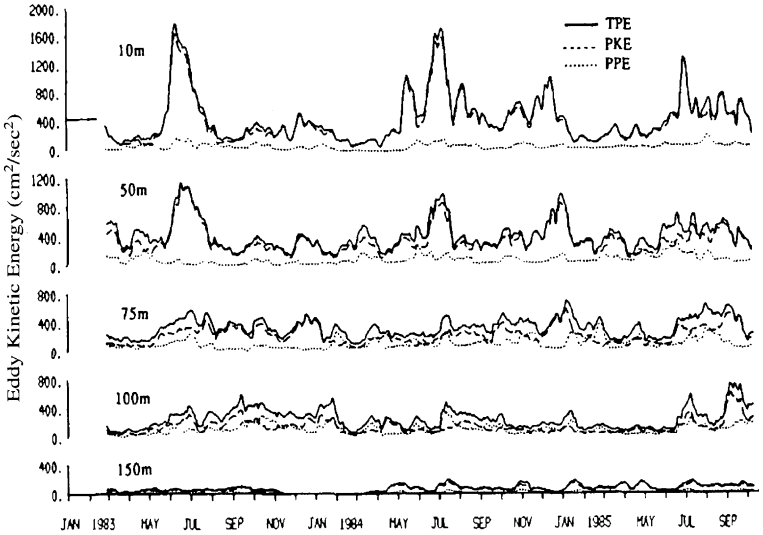

Fig. 5. The eddy kinetic energy on the equator at 28°W, adapted from WW. The eddy potential energy (PPE) is negligible, the total eddy energy (TPE, —) is almost identical with the eddy kinetic energy (PKE).

of temperature and velocity (Weisberg and Colin, 1986). Accordingly, the 32 month records on the equator at 28°W show interannual variability in TIW strength (Fig. 5). This observed range of variability of ±30% can be interpreted as uncertainty by which to judge the performance of the numerical model.

On the equator at 28°W the TIWs start developing in May and reach their maximal energy in July with an energy peak of 1600 cm^2/s^2 at the surface and 600 cm^2/s^2 at 75 m depth; the potential energy of the TIWs is negligible by comparison (Fig. 5). The TIWs become weaker in the fall but

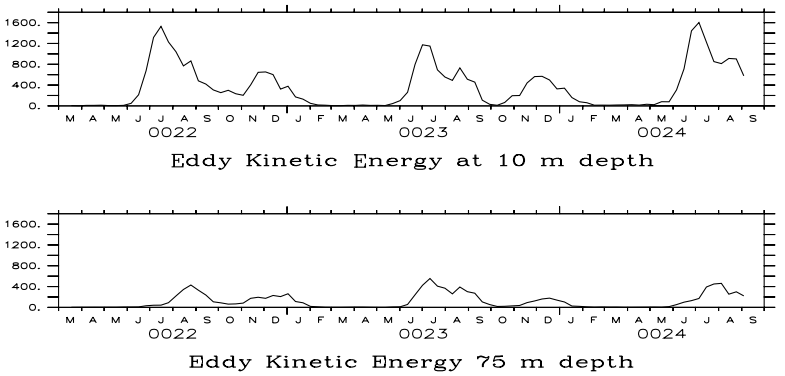

Fig. 6. The eddy kinetic energy on the equator at 28°W in the model (in cm^2/s^2).

gain in strength again in December before they vanish in February/March. For the comparison the eddy kinetic energy (EKE) in the model is defined as in WW:

$$\mathrm{var}(\mathbf{u}) = (\langle u'u' \rangle + \langle v'v' \rangle)/2,$$

where the angle brackets denote an average over 30 days and the primes denote deviations about the 30 days average. This method of computing the energy retains the temporal evolution of the velocity field but energy of frequency bands adjacent to the TIW frequency, especially of higher frequencies, will show up in this variance. This will lead to a systematically lower energy in the model, because the model lacks by construction the high frequency component of the wind field. Nevertheless, apart from the absence of background noise, the behaviour of the model mirrors the observations (Fig. 6). Not only does the model produce TIWs of the right strength but it also captures the right onset and end of the TIW season. Furthermore, in the model as in the observations (Weisberg et al., 1987) the kinetic energy is evenly partitioned between the meridional and the zonal component (not shown). Notice that in the model the TIW strength and their onset varies from year to year, although the model is forced with climatological winds. The onset is always in May, in phase with the spin-up of the EUC and the equatorial gyre (Anderson and Corry, 1985); but the first TIWs can appear anytime between the beginning and the end of May (Fig. 6). This is indicative of a chaotic behaviour of TIWs. This differs from the findings of Vialard et al. (2003), who find in a numerical study of the Pacific Ocean that the phase of the TIWs is locked to the seasonal cycle and is insensitive to the initial conditions. The different behaviour of the two model solutions is possibly due to their difference in viscosity. In fact, Vialard et al. (2003) show that increasing the wind stress by 50% (which like reducing friction can turn a limit cycle into chaos) leads to a random onset of TIW activity.

From the comparisons above one can see that at the equator at 28°W the model realistically reproduces the TIWs. The 32 month record that is used for this comparison is unique in its duration, all the other relevant records are shorter and cover one year at most. Still, even the shorter data sets yield information about the spatial extent of the TIWs and will be listed here to corroborate the model results.

At the surface, the TIWs are generally confined to regions west of 8°W (WW, Steger and Carton, 1991). Within the limits of the uncertainty, the TIW energy is constant between 28°W and

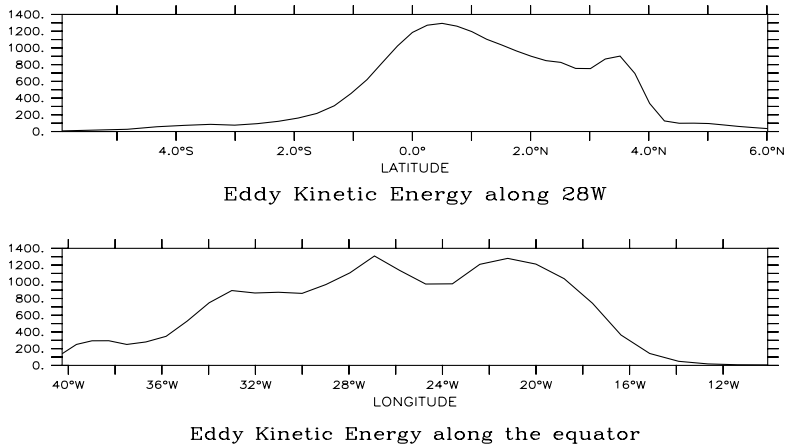

Fig. 7. The eddy kinetic energy of the velocity at the surface in July along 28°W (upper figure, in cm^2/s^2) and along the equator (lower figure).

15°W; along the 28°W meridian the wave energy has a maximum between 0.75°S and 0.75°N (WW). Observations at 1.75°N and 3°N indicate an energy level of at least 50% of the maximum (WW). No TIWs could be observed at 28°W/6°N (WW). The maximum energy in the model, like in the observations, is on the equator and drops off significantly beyond 3°N (Fig. 7, top). The main difference between the observations and the model results is that in the model the energy dropps off east of 20°W whereas in the observations the energy level decreases somewhere between 15°W and 8°W (Fig. 7, bottom).

There are four more observations that provide information about the extent of the TIWs and the model results are consistent with each of them.

- On the equator at 4°W at 600 m depth, during summer and fall Weisberg et al. (1979) find a variance of the meridional velocity of 30 cm^2/s^2 in the 20–40 day band. The respective model value is 20 cm^2/s^2.
- During the summer of 1974, at 15°N/28°W, Weisberg et al. (1980) find at 320 m depth a wave with a period of approximately 1 month and an amplitude of the meridional velocity perturbation of 10 cm/s. The records do not show a wave of this period at 1050 m depth. Both observations are reproduced in the model.
- On the equator at the western boundary, the observations by Schott et al. (1993) suggest for the band of 20–50 days a velocity variance of 40 cm^2/s^2, identical to the model value.
- Boebel et al. (1999) show the trajectory of a SOFAR float that, during winter 1994 at 800 m depth, between 40°W and 25°W, outlines a wave with a wavelength of approximately 800 km and a period of approximately one month. From Fig. 3 of Boebel et al. (1999) the authors infer a perturbation of the meridional velocity of a few cm/s. For comparison, the intermediate flow field in the model during November is shown in Fig. 8. One can see the circular velocity signals of the TIWs superimposed on the westward flow of a seasonal Rossby wave (see Jochum and Malanotte-Rizzoli (2003b) for a detailed discussion of the intermediate flow). Similar to the

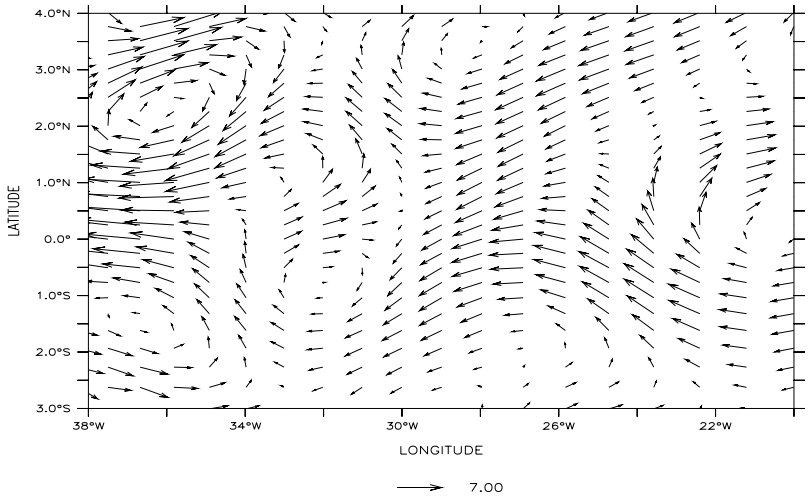

Fig. 8. The flow field in the model at 700 m depth during November.

observations, the TIWs in the model produce at these depths velocity perturbations of a few cm/s.

- An altimetry study by Musman (1992) demonstrates that the surface signal of the TIWs resembles Yanai waves that are slightly stronger in the north than the south and extend from 7°S and 7°N. The model results, too, resemble a Yanai wave (Fig. 9) which is stronger north of the equator than south of it.

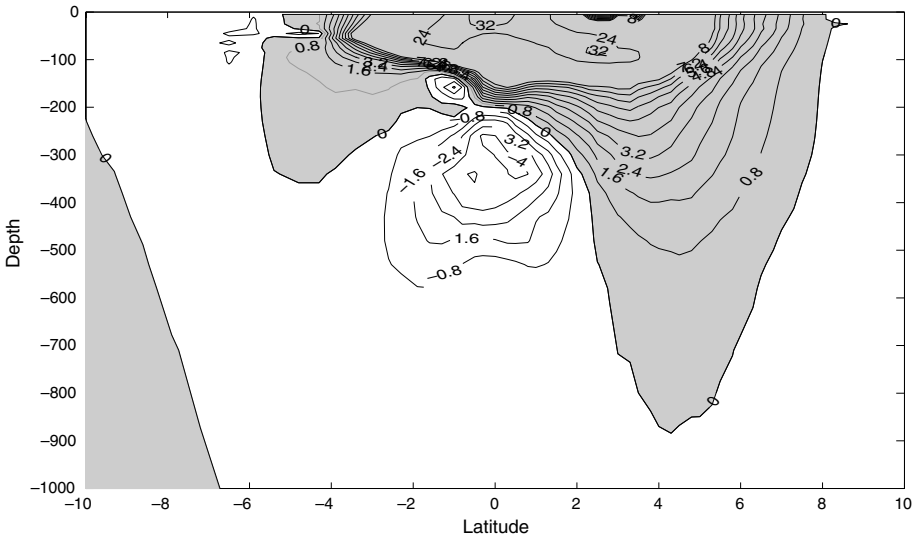

Fig. 9. The first empirical orthogonal function of the highpass filtered meridional velocity at 20°W. It explains 51% of the variance, the second EOF explains 19% of the variance. The numbers indicate the meridional velocity (in cm/s) and areas of positive values are shaded. Note the two different contourline intervals. The strong cross-equatorial flow in the surface is the signature of a Yanai wave (Matsuno, 1966).

This section provided a review of the observations of TIWs in the Atlantic and compares them with the present model results. The observations show that the TIWs exist on both sides of the equator and are generated from May to January. Their wavelength can be as long as 1200 km and as short as 600 km, their period is centered at 25 days. The energy of the TIWs is centered on the equator and trapped near the surface in the center of the basin, but weak signals in the 20–40 day band have been detected along the equator at the western boundary, at 4°W, and all along the equator in the intermediate water. The comparisons with the model results show that the TIWs in the model have properties and amplitudes that the match the observed TIWs. The spatial extent of the TIW is reproduced as well, with the exception of their easternmost extent at the surface which falls short of the observed extent by some 500 km.

3. Energetics of the TIWs

The previous section demonstrates that the TIWs are adequately represented in the present numerical model but that the observations are too few to analyze the TIW energetics in detail. Therefore, in this section the model results are used to describe how the TIWs are generated in the Atlantic and what their velocity and temperature structure is.

Fig. 10 shows the annual mean EKE in the 20–50 day band at 10 m depth. Here, EKE is defined as $(u'^2 + v'^2)/2$, the primed terms being the deviation from the annual mean. The EKE is centered at the equator and does barely reach to the western boundary. The second maximum at the northwestern corner of the displayed domain is due to the barotropic instability of the north equatorial countercurrent. This instability is not related to the TIWs as discussed in Jochum and Malanotte-Rizzoli (2003c). Fig. 11 shows the EKE in the 20–50 day band along the equator. The energy is largely confined to the upper 100 m. To understand the sources and sinks of TIW energy, a technique is used that is similar to that of Masina et al. (1999). Starting from the equations of

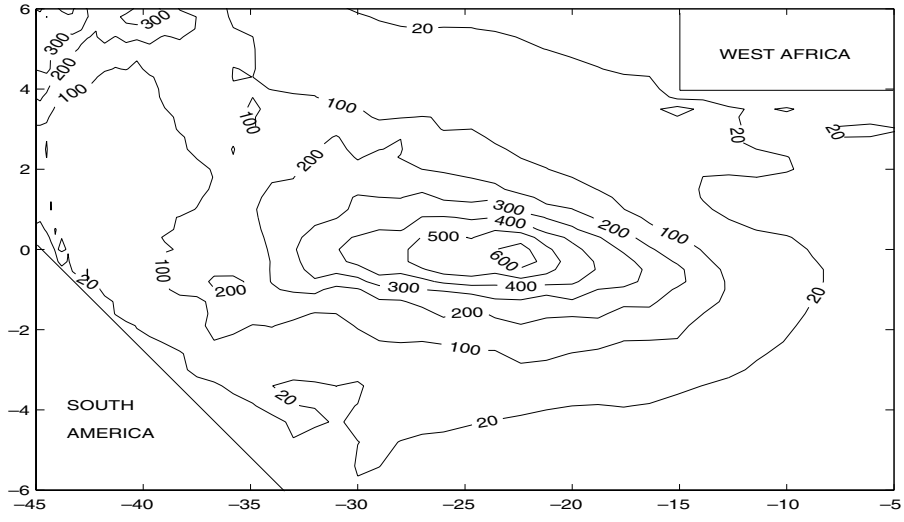

Fig. 10. The annual mean eddy kinetic energy at 10 m depth in the 20–50 day band (in cm^2/s^2).

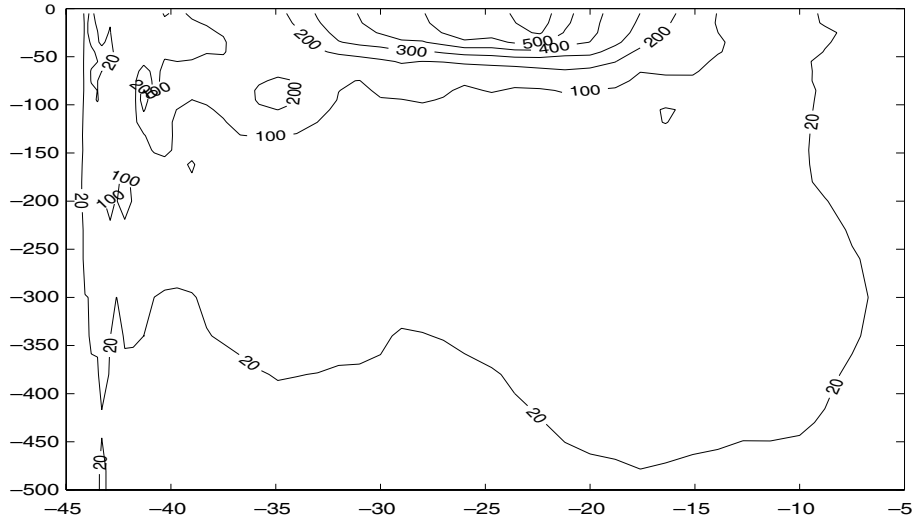

Fig. 11. The annual mean eddy kinetic energy along the equator in the 20–50 day band (in cm^2/s^2).

motion, they derive a time mean budget for EKE that can be evaluated with the results of a numerical model:

$$\underset{(1)}{\vec{U}\cdot\vec{\nabla}K_{\mathrm{e}}}+\underset{(2)}{\overrightarrow{u'}\cdot\vec{\nabla}K_{\mathrm{e}}}=-\vec{\nabla}\cdot\underset{(3)}{(\overrightarrow{u'}p')}-\underset{(4)}{g\rho'w'}+\rho_{\mathrm{o}}[\underset{(5)}{-\overrightarrow{u'}\cdot(\overrightarrow{u'}\cdot\vec{\nabla}\vec{U})}+\underset{(6)}{A_{\mathrm{h}}\overrightarrow{u'}\cdot\nabla^2\overrightarrow{u'}}+\underset{(7)}{\overrightarrow{u'}\cdot(A_{\mathrm{v}}\overrightarrow{u'}_z)_z}]. \tag{1}$$

The capital letters denote annual mean values, the primes the deviation from the annual mean. K_{e} stands for EKE, (u, v, w) is the velocity vector, p the pressure, ρ the density, g the acceleration due to gravity and A_{h} and A_{v} the horizontal and vertical viscosity. Sources for the TIW energy could be conversion from mean kinetic energy to EKE (barotropic conversion, 5) or conversion from mean potential energy to EKE (baroclinic conversion, 4). The physical mechanisms that lead to barotropic or baroclinic conversion are commonly referred to as barotropic or baroclinic instability. Lindzen (1988) and Proehl (1996) argue that for complicated flow structures the distinction between barotropic and baroclinic instability becomes meaningless, instead they introduce the concept of over-reflection. We, the authors, are not quite convinced that the traditional instability concepts are not useful, but the interested reader is referred to their original works for a detailed discussion of their ideas.

The EKE resulting from the instabilities can be advected (1,2) or radiated away (3), returned to the mean flow (4,5), or dissipated (6,7). In principle, a correlation between the wind stress and the surface velocity is an additional energy source or sink for TIWs, but the model's prescribed climatological wind stress does not allow for a feedback between wind and SST. This makes, at least in the model, the wind contribution to the TIW energy budget negligible. Recent observations in the Pacific showed that there is a correlation between SST and the wind curl (Chelton et al., 2001). From these observations, it does not appear that this translates into a systematic correlation between the surface flow and the wind stress over the domain of the TIWs. However, this has to

be explored in more detail; for the present study it is argued that the model results are consistent with the available observations of TIWs and therefore the model properly accounts for the most important sources and sinks of TIW energy.

For the following analysis the model results have been highpass filtered to remove variability with periods of more than 60 days. Fig. 12 shows the different source terms averaged over the unstable area (the upper 150 m from 40°W to 10°W). The barotropic conversion of the zonal flow $(-\rho_o \overline{u'v'} U_y)$ is the dominating source for TIW energy; the remaining deformation terms $\left(-\rho_o \left(\overline{u'u'} U_x + \overline{u'v'} V_x + \overline{v'v'} V_y\right)\right)$ and baroclinic conversion $(-g\overline{\rho' w'})$ are much less important. The small but not negligible amount of baroclinic conversion along 2 °N can explain the asymmetry in the TIW strength (Figs. 9 and 10). The present results are similar to the results of Cox (1980) but different from the results of Masina et al. (1999), who find that baroclinc instability is the largest source of TIW energy in the Pacific. Two possibilities could account for this difference: The dynamics of the Pacific TIWs could indeed be different than that of the Atlantic TIWs, or the higher viscosity in the Masina et al. (1999) experiments removes the strong current shears that are necessary for barotropic instability.

Fig. 13 shows the dominating source of TIW energy, the barotropic conversion rate $\left(-\rho_o \overline{u'v'} U_y\right)$, along the equator. It is confined to the upper 100 m and extends from 36°W to 16°W. The location and the spatial pattern of the barotropic conversion matches the spatial pattern of the curvature of the mean zonal flow between EUC and nSEC. Because $u_{yy} > \beta$ is a necessary condition for barotropic instability, this is further indication that barotropic instability of the EUC/nSEC is the main energy source for the TIWs.

Comparison of Fig. 12 with Fig. 10 and of Fig. 13 with Fig. 11 shows that the spatial distribution of TIW energy is largely identical to the distribution of its sources—both seem to extend approximately from 36°W to 16°W and from 2°S and 3°N and are mainly confined to the upper 100 m. Plumb (1983) pointed out that the distinction between flux terms and conversion terms in Eq. (1) is ambiguous so that a *local* analysis of individual terms can be misleading. Therefore it is important to note that the conclusion, that the energy source for the TIWs is barotropic and not baroclinic conversion, is based on an *integral* budget over the domain of high EKE. Furthermore,

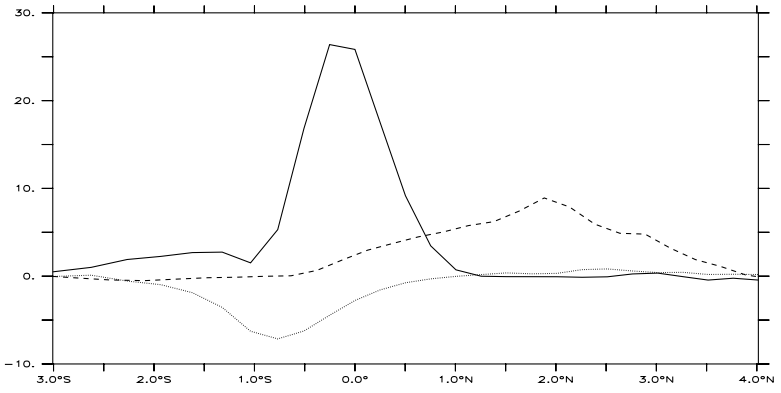

Fig. 12. The energy conversion rates (in 10^{-6} kg/ms^3) averaged over the upper 150 m, from 40°W to 10°W. Shown is the barotropic conversion of the zonal flow (—), baroclinic conversion (- - -) and the remaining deformation terms (. . ., see text). The vertical and zonal structure of the barotropic conversion can be seen in Fig. 13.

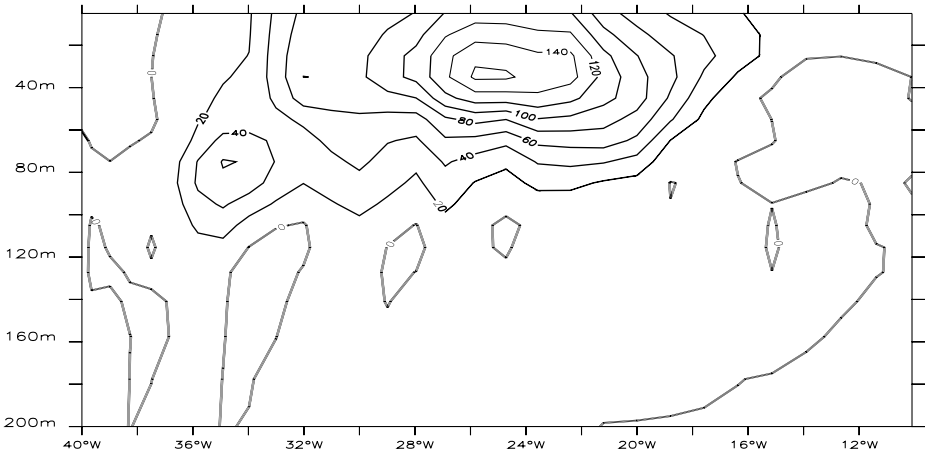

Fig. 13. The barotropic conversion rate of the zonal flow along the equator (in 10^{-6} kg/ms^3). The strength and spatial structure of the conversion rate matches the ones of the curvature of the zonal flow (u_{yy}, not shown).

the similar spatial structure of EKE, the curvature of the zonal flow and the barotropic conversion rate shows that the present interpretation of Eq. (1) is physically meaningful.

Besides the conversion of energy from the mean to eddy fields, there are potentially additional sources and sinks: advection, viscosity and radiation. The model results show that neither advection nor horizontal viscosity make a significant contribution to the energy budget. In the present study of the Atlantic TIWs, in the box between 40°W and 10°W and 2°S and 3°N and between the surface and 150 m depth, the instabilities produce 2.1×10^9 W (GW) of EKE. A substantial part of this energy, 1.1 GW, is dissipated immediately within the equatorial mixed layer by the vertical viscosity. The remainder of the TIW energy is radiated out of the box by TIWs, 0.2 GW downwards, below the thermocline and 0.6 GW polewards (see Fig. 14). The remainder of the budget is contributed by minor terms with contributions of less than 0.1 GW. This budget is consistent with WW's observations along the equator at 28°W, who find that

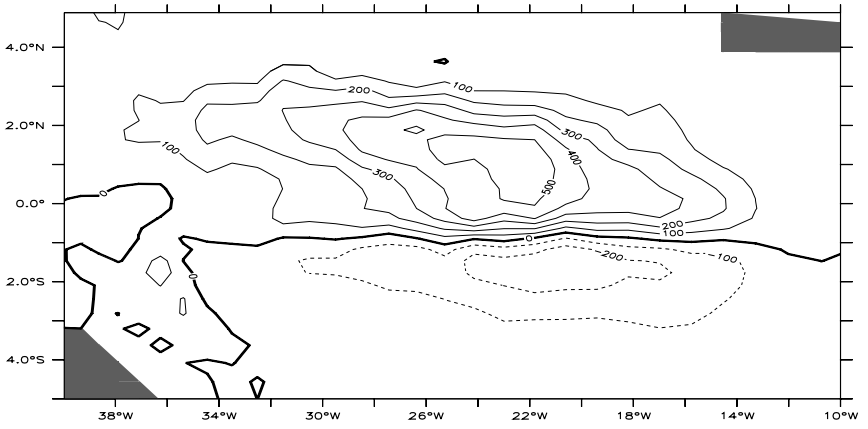

Fig. 14. The meridional radiation of TIW energy (or pressure flux divergence) averaged over the upper 150 m of the water column (in kg/ms^3).

baroclinc instability is negligible compared to barotropic instability and that meridional radiation of energy is the largest quantifiable sink of TIW energy. They did not provide an estimate for dissipation.

The free equatorial waves available for the energy radiation have been discussed in great detail by Cox (1980). Given their range in frequency and wave length, the TIW energy can only project on Yanai waves and Rossby waves of the meridional modes 1 and 2. The Yanai waves have an eastward and downward group velocity, the Rossby waves have a downward velocity as well but a group velocity that could be eastward or westward, depending on the exact frequency and wavenumber. It is the function of the eddy pressure flux divergence (or radiation) shown in Fig. 14 to move energy from the very narrow EKE generation region poleward to create the meridional structure of the Yanai and Rossby waves (see also Philander (1990) for the generation of latitudinal standing modes at the equator). Of course, it is not clear to what extent the free equatorial waves in the Atlantic resemble the analytically derived structures of Yanai and Rossby waves. The sheared background flow, the presence of bottom topography and the strong diabatic interaction with the mixed layer should distort the linear waves; moreover the mean and the wave induced velocities are strong enough to lead to a coupling of wave and mean flow. However, east of the unstable region at 4°W both, the observations (Weisberg et al., 1979) and the present model results clearly show a wave whose wavelength and phase and group speed indicate a Yanai wave. West of 15°W the solution is nonlinear and it is not possible anymore to isolate the energy of each wave by mode decomposition. One can, however, get a general idea of the structure of the planetary waves from a cross-section like Fig. 9. Most of the signal is within several degrees of the equator and in the upper 150 m of the water coloumn, but the TIW can reach into the intermediate layer and extend more than 5° poleward of the equator.

The present analysis of the energetics of the TIWs shows that the TIWs are created mainly along the equator by the barotropic instability of the EUC/nSEC. About half of this energy is dissipated locally, the other half is radiated polewards and downwards. These results are consistent with the observations of WW and the numercial study of Cox (1980). The next section will investigate the heat flux of the TIWs.

4. Heat flux of the TIW

The previous section shows that the TIW energy is largely confined to the equatorial upper thermocline. To the extent that the instabilities are projected on linear free equatorial waves, their heat flux is necessarily small because linear planetary waves do not generate a time mean heat flux. Therefore, the present focus is the TIW heat flux in the mixed layer, where the large amplitudes of the TIWs and the diabatic processes within the mixed layer could lead to a meridional heat flux. If the TIW induced meridional heat flux is comparable to the atmospheric heat flux, the TIWs have to be accounted for in climate studies. Hansen and Paul (1984) were the first to show with an analysis of drifter data in the equatorial Pacific that the meridional heat flux of TIWs is comparable to the atmospheric heat flux.

Here, eddies are defined as deviation from the annual mean, so that the eddy heat fluxes have seasonal and a subseasonal component. The first is associated with the seasonally changing wind field and the second is caused by the TIWs. A spectral analysis shows that approximately 70% of

the eddy heat flux is due to TIWs. This is a result reminicent of Hazeleger et al. (2001), who find that in the equatorial Pacific the TIWs are responsible for most of the eddy mass transport.

The time mean temperature equation is given by

$$\bar{u}\overline{T}_x + \bar{v}\overline{T}_y + \bar{w}\overline{T}_z = -\overline{(u'T')}_x - \overline{(v'T')}_y - \overline{(w'T')}_z + (k_h\overline{T}_x)_x + (k_h\overline{T}_y)_y + (k_v\overline{T}_z)_z + \frac{1}{\rho c_p h}\overline{H}f, \tag{2}$$

where the overbars denote the annual mean and the primes the deviation from it. Hf is the atmospheric heat flux (in W/m^2) and k_h and k_v are the horizontal and vertical diffusion coefficients, respectively. ρ is the density and c_p the heat capacity of seawater, h is the mixed layer depth, set to be 20 m. At 20°W, the model results show that the zonal derivatives are not important, neither is the meridional diffusion. For Fig. 15 the temperature equation is multiplied by $\rho c_p h$ to make it easier to relate the oceanic fluxes to the atmospheric fluxes. The figure shows the most important terms of the heat budget of the upper 20 m at 20°W. The atmospheric heat flux is mainly diffused down into the thermocline and advected northward by the mean flow. The heat flux due to upwelling and eddies are important but clearly not dominating the budget. More importantly, this figure shows that the meridional eddy heat flux divergence is largely compensated for by the vertical eddy heat flux divergence. This is a very surprising result because all studies that the authors are aware of (e.g. Hansen and Paul, 1984 , WW, Swenson and Hansen, 1999) suggest that the TIWs, the largest component of the eddy heat flux divergence, are an important part of the equatorial mixed layer heat budget.

The neglect of the compensating vertical eddy heat flux might have two reasons. First, it is simply impractical to observe the vertical eddy heat flux and second, the vertical eddy heat flux is indeed negligible away from the equator. Simple scaling suggest that the ratio between vertical and meridional eddy heat flux is of the order:

$$O\left(\frac{(w'T')_z}{(v'T')_y}\right) = \frac{\beta L}{f}$$

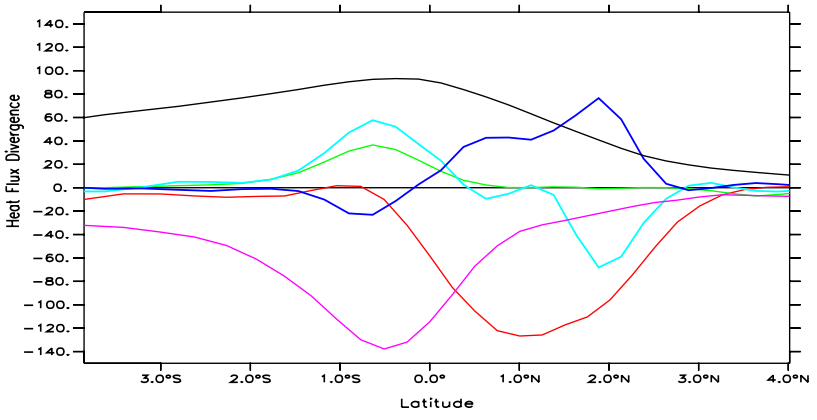

Fig. 15. The different components of the heat flux divergence of the upper 20 m along 20°W (in W/m^2). Atmosphere: black; downward diffusion: purple; mean northward transport: red; upwelling: green; meridional eddy flux: light blue; vertical eddy flux: dark blue.

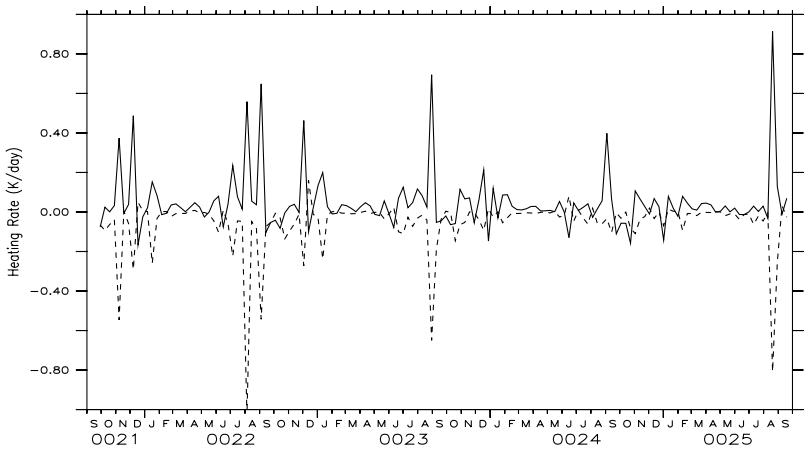

Fig. 16. The heating tendency induced by the meridional eddy flux divergence ($(v'T')_y$, —) and the vertical eddy flux divergence ($(w'T')_z$, - - -).

which is small in mid-latitudes but equals 1 near the equator. This compensation, however, explains a curious fact about El Niño forecasts: Although the forecast models are based on linear ocean dynamics without TIWs, their skills are remarkably good. This has been pointed out already by Vialard et al. (2001), who suspected that vertical compensation might be relevant. The present study shows that the vertical heat flux is indeed very important and is locally even more important than the meridional heat flux. This compensation is not only a phenomenon of the annual mean but is a part of the instabilities as can be seen in Fig. 16. The anticorrelation between meridional and vertical heat flux is obvious. This compensation leaves an heating rate between 0.1

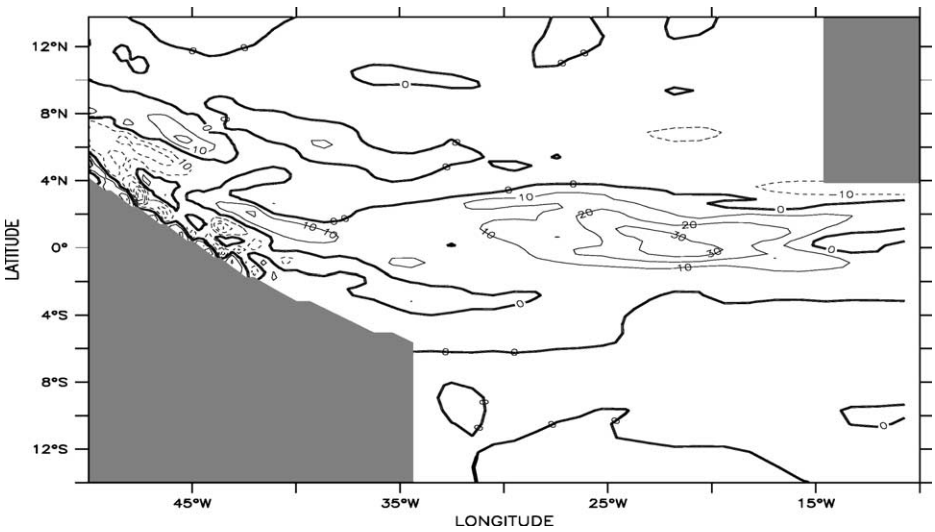

Fig. 17. The total eddy heat flux divergence in the upper 20 m, averaged over the summer months (May to September; in W/m^2).

and 0.2 K/day which, together with the TIW periods of 30–40 days, is sufficient to explain the observed TIW induced SST anomalies of approximately 2–3 °C. The resulting annual eddy heat flux divergence is small and even during the summer, it does not exceed 30 W/m^2 in the upper 20 m (Fig. 17).

5. Summary and discussion

A numerical model of the tropical Atlantic is used to analyze the properties of the Atlantic TIWs. The comparison with the observations shows that the model realistically represents the TIWs. The model results were then used to analyze the TIWs in detail, which is not possible with observations alone. This analysis demonstrates that the TIWs extend several degrees poleward of each side of the equator and that they are generated between May and January. The often heard notion that the Atlantic TIWs are limited to the north of the equator and only appear during summer is based solely on satellite infrared observations. During summer, the strong SST front at 2°N makes it easy to detect the TIWs, but this study shows that the TIWs are present throughout most of the year, even south of the equator.

The analysis of the TIW energetics leads to the conclusion that barotropic instability of the EUC/nSEC is the main generation mechanism for Atlantic TIWs, suggesting that a small numerical horizontal viscosity is crucial for the appropriate representation of TIWs in models. Approximately half of the TIW energy is immediately dissipated in the mixed layer by vertical dissipation. The remainder of the energy is largely projected on free equatorial waves and radiated downwards and polewards. Surprisingly, the TIWs are not as important for the mixed layer heat budget as hitherto assumed. The numerical model revealed that the large meridional heat flux which is reported in the literature is mostly compensated by the vertical heat flux of the TIWs. In the present model, the average heat convergence in the mixed layer between 40°W and 10°W, and between 2°S and 3°N during the summer amounts to approximately 10 W/m^2.

The process of vertical cancellation is a robust result because it agrees with the predictions of linear wave theory. The exact value of the cancellation, however, has to be interpreted with care. As discussed earlier, the waves are not always linear; more importantly though, the model does not properly resolve the equatorial mixed layer and the SST is restored to a prescribed value. Therefore it is doubtful that the present model adequately represents ocean–atmosphere interaction. For example, Vialard (pers. comm.) reports that in his model of the tropical Pacific, which has the same vertical resolution and the same boundary conditions as the present model, the vertical compensation is only 20–30% of the meridional heat flux. Further research will be needed to understand the details of ocean–atmosphere interaction in the presence of TIWs. This future research will need improved upper boundary conditions, like the interactive heat flux formulation by Seager et al. (1995) which locally computes the atmospheric heat flux from winds and SST.

Although their contribution to the mixed layer heat budget appears to be much smaller than expected and smaller than the observational uncertainties in the atmospheric heat flux, the TIWs are not unimportant. Consistenly applying 10 W/m^2 to the mixed layer over the summer will lead to a heating of 1 K, enough to remove the 'cold bias' in tropical ocean models (Murtugudde et al., 1996). The TIWs have a dynamical impact on the equatorial circulation as well: They remove kinetic energy from the EUC and dissipate it in the equatorial thermocline. This slows down the

EUC and removes a part of the mechanical energy input of the wind (Hansen and Paul, 1984); furthermore, the Eliassen-Palm flux of the TIWs drives the equatorial subsurface undercurrents (Jochum and Malanotte-Rizzoli, 2003a). And last but not least, because of their associated strong velocities, a detailed understanding of their structure is necessary to plan and interpret observational campaigns along the equator.

Acknowledgements

The authors benefitted from the helpful suggestions of Alan Plumb, Raffaele Ferrari, Xiaoyun Zang, Baylor Fox-Kemper, Jerome Vialard and one anonymous reviewer. The computations have been performed at the NCAR facilities in Colorado and this research was funded with NOAA grant Nr NA16GP1576 at MIT.

References

Anderson, D.L.T., Corry, R.A., 1985. Seasonal transport variations in the Florida straits: a model study. J. Phys. Oceanogr. 15, 773–786.

Boebel, O., Schmid, C., Zenk, W., 1999. Kinematic elements of Antarctic intermediate water in the south Atlantic. Deep Sea Res. 46, 355–392.

Bryden, H., Brady, E., 1989. Eddy momentum and heat fluxes and their effects on the circulation of the equatorial Pacific Ocean. J. Mar. Res. 47, 55–79.

Chelton, D.B., Wentz, F.J., Gentemann, C.L., de Szoeke, R.A., Schlax, M.G., 2000. Satellite microwave SST observations of transequatorial tropical instability waves. Geophys. Res. Lett. 27, 1239–1242.

Chelton, D.B., Esbensen, S.K., Schlax, M.G., Thum, N., Freilich, M.H., Wentz, F.J., Gentemann, C.L., McPhaden, M., Schopf, P.S., 2001. Observations of coupling between surface wind stress and sea surface temperature in the eastern Tropical Pacific. J. Climate 14, 1479–1498.

Cox, M., 1980. Generation and propagation of 30-day waves in a numerical model of the Pacific. J. Phys. Oceanogr. 10, 1168–1186.

Dueing, W., Hisard, P., Katz, E., Knauss, J., Meincke, J., Miller, L., Moroshkin, K., Philander, G., Rybnikov, A., Voigt, K., Weisberg, R., 1975. Meanders and long waves in the equatorial Atlantic. Nature 257, 280–284.

Hansen, D., Paul, C., 1984. Genesis and effects of long waves in the equatorial Pacific. J. Geophys. Res. 89, 10431–10440.

Hazeleger, W., deVries, P., vanOldenborgh, G., 2001. Do tropical cells ventilate the Indo-Pacific equatorial thermocline? Geophys. Res. Lett. 28, 1763–1766.

Hellerman, S., Rosenstein, M., 1983. Normal monthly wind stress over the world ocean with error estimates. J. Phys. Oceanogr. 13, 1093–1104.

Hisard, P., Henin, C., Houghton, R., Piton, B., Rual, P., 1986. Oceanic conditions in the tropical Atlantic during 1983 and 1984. Nature 322, 243–245.

Jochum, M., Malanotte-Rizzoli, P., 2003a. A new driving mechanism for the south equatorial undercurrent. J. Phys. Oceanogr.

Jochum, M., Malanotte-Rizzoli, P., 2003b. On the flow of Antarctic intermediate water along the equator. In: Interhemispheric Water Exchanges in the Atlantic Ocean. Elsevier Series.

Jochum, M., Malanotte-Rizzoli, P., 2003c. On the generation of North Barzil current rings. J. Mar. Res. 61/2, 147–162.

Katz, E., 1997. Waves along the equator in the Atlantic. J. Phys. Oceanogr. 27, 2536–2544.

Legeckis, R., 1977. Long waves in the eastern equatorial Pacific Ocean: a view from a geostationary satellite. Science 197, 1179–1181.

Legeckis, R., Reverdin, G., 1987. Long waves in the equatorial Atlantic Ocean during 1983. J. Geophys. Res. 92, 2835–2842.

Lindzen, R., 1988. Instability of plane parallel shear flow. Pure Appl. Geophys., 126.
Masina, S., Philander, S., 1999. An analysis of tropical instability waves in a numerical model of the Pacific Ocean—1. Spatial variability of the waves. J. Geophys. Res. 104, 29613–29635.
Masina, S., Philander, S., Bush, A., 1999. An analysis of tropical instability waves in a numerical model of the Pacific Ocean—2. Generation and energetics of the waves. J. Geophys. Res. 104, 29613–29635.
Matsuno, T., 1966. Quasi-geostrophic motions in equatorial areas. J. Meteorol. Soc. Jpn. 2, 25–43.
Menkes, C., Kennan, S., Flamant, P., et al., 2002. A whirling ecosystem in the equatorial Atlantic. Geophys. Res. Lett. 29 (48), 1–4.
Murtugudde, R., Seager, R., Busalacchi, A., 1996. Simulation of the tropical oceans with and ocean GCM coupled to an atmospheric mixed layer model. J. Climate 9, 1796–1815.
Musman, S., 1992. Geosat altimeter observations of long waves in the equatorial Atlantic. J. Geophys. Res. 97, 3573–3579.
Philander, S., 1976. Instabilities of zonal equatorial currents—Part 1. J. Geophys. Res. 81, 3725–3735.
Philander, S., 1978. Instabilities of zonal equatorial currents—Part 2. J. Geophys. Res. 83, 3679–3682.
Philander, S., 1990. El Nino, La Nina and the Southern Oscillation. Academic Press.
Philander, S., Hurlin, W., Pacanowski, R., 1986. Properties of long equatorial waves in models of the seasonal cycle in the tropical Atlantic and Pacific Oceans. J. Geophys. Res. 91, 14207–14211.
Plumb, R., 1983. A new look at the energy cycle. J. Atmos. Sci. 40, 1669–1688.
Proehl, J., 1996. Linear instability of equatorial zonal flows. J. Phys. Oceanogr. 26, 601–621.
Richardson, P., Philander, S., 1987. The seasonal variations of surface currents in the tropical Atlantic Ocean: a comparison of ship drift data with results from a general circulation model. J. Geophys. Res. 92, 715–724.
Richardson, P., Reverdin, G., 1987. Seasonal cycle of velocity in the Atlantic NECC as measured by surface drifters, current meters and ship drifts. J. Geophys. Res. 92, 3691–3708.
Schott, F., Fischer, J., Reppin, J., Send, U., 1993. On mean and seasonal currents and transports at the western boundary of the equatorial Atlantic. J. Geophys. Res. 98, 14353–14368.
Seager, R., Blumenthal, M., Kushnir, Y., 1995. An advective atmospheric mixed layer model for ocean modeling purposes: global simulation of atmospheric heat-fluxes. J. Climate 8, 1951–1964.
Steger, J., Carton, J., 1991. Long waves and eddies in the tropical Atlantic Ocean: 1984–1990. J. Geophys. Res. 96, 15161–15171.
Swenson, M., Hansen, D., 1999. Tropical Pacific Ocean mixed layer heat budget: the Pacific cold tongue. J. Phys. Oceanogr. 29, 83–91.
Vialard, J., Menkes, C., Boulanger, J., Delecluse, P., Guilyardi, E., McPhaden, M., Madec, G., 2001. A model study of oceanic mechanisms affecting equatorial Pacific sea surface temperature during the 1997–1998 El Nino. J. Phys. Oceanogr. 31, 1649–1675.
Vialard, J., Menkes, C., Anderson, D., Balmaseda, M., 2003. Sensitivity of Pacific Ocean tropical instability waves to initial conditions. J. Phys. Oceanogr. 33, 105–121.
Weisberg, R., 1984. Instability waves observed on the equator in the Atlantic Ocean during 1983. Geophys. Res. Lett. 11, 753–756.
Weisberg, R., Colin, C., 1986. Equatorial Atlantic Ocean temperature and current variations during 1983 and 1984. Nature 322, 240–243.
Weisberg, R., Weingartner, T., 1988. Instability waves in the equatorial Atlantic Ocean. J. Phys. Oceanogr. 18, 1641–1657.
Weisberg, R., Horigan, A., Colin, C., 1979. Equatorially trapped Rossby-gravity wave propagation in the Gulf of Guinea. J. Mar. Res. 37, 67–86.
Weisberg, R., Miller, L., Horigan, A., Knauss, J., 1980. Velocity observations in the equatorial thermocline during GATE. Deep-Sea Res. 26 (Suppl. II), 217–248.
Weisberg, R., Hickman, J., Tang, T., Weingartner, T., 1987. Velocity and temperature observations during the seasonal response of the equatorial Atlantic experiment at 0N, 28W. J. Geophys. Res. 92, 5061–5075.
Yu, Z., McCreary, J., Proehl, J., 1995. Meridional asymmetry and energetics of tropical instability waves. J. Phys. Oceanogr. 25, 2997–3007.